International Journal of Mycobacteriology 5 (2016) 66–73

HOSTED BY

Available at www.sciencedirect.com

ScienceDirect

journal homepage: www.elsevier.com/locate/IJMYCO

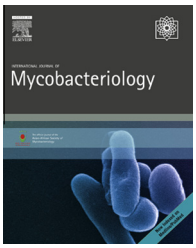


# Populations of latent *Mycobacterium tuberculosis* lack a cell wall: Isolation, visualization, and whole-genome characterization

*Ali Akbar Velayati* [a], *Thomas Abeel* [b,c], *Terrance Shea* [b], *Gennady Konstantinovich Zhavnerko* [d], *Bruce Birren* [b], *Gail H. Cassell* [e], *Ashlee M. Earl* [b], *Sven Hoffner* [f], *Parissa Farnia* [a,*]

[a] *Mycobacteriology Research Centre, National Research Institute of Tuberculosis and Lung Disease (NRITLD), Shahid Beheshti University of Medical Sciences, Tehran, Iran*

[b] *Genome Sequencing & Analysis Program, The Broad Institute of MIT & Harvard, Cambridge, MA, USA*

[c] *Delft Bioinformatics Lab, Delft University of Technology, Delft, The Netherlands*

[d] *The Republican Research and Practical Centre for Epidemiology and Microbiology, Minsk, Belarus*

[e] *Department of Global Health and Social Medicine, Harvard Medical School, Boston, MA, USA*

[f] *Department of Microbiology, The Public Health Agency of Sweden, Solna, Sweden*

ARTICLE INFO

*Article history:*
Received 7 November 2015
Received in revised form
28 November 2015
Accepted 9 December 2015
Available online 28 December 2015

*Keywords:*
*Mycobacterium tuberculosis*
Tuberculosis latency
Whole-genome sequencing

ABSTRACT

*Objective/Background:* *Mycobacterium tuberculosis* (MTB) causes active tuberculosis (TB) in only a small percentage of infected people. In most cases, the infection is clinically latent, where bacilli can persist in human hosts for years without causing disease. Surprisingly, the biology of such persister cells is largely unknown. This study describes the isolation, identification, and whole-genome sequencing (WGS) of latent TB bacilli after 782 days (26 months) of latency (the ability of MTB bacilli to lie persistent).

*Methods:* The *in vitro* double-stress model of latency (oxygen and nutrition) was designed for MTB culture. After 26 months of latency, MTB cells that persisted were isolated and investigated under light and atomic force microscopy. Spoligotyping and WGS were performed to verify the identity of the strain.

*Results:* We established a culture medium in which MTB bacilli arrest their growth, reduce their size (0.3–0.1 μm), lose their acid fastness (85–90%) and change their shape. Spoligopatterns of latent cells were identical to original $H_{37}R_v$, with differences observed at spacers two and 14. WGS revealed only a few genetic changes relative to the already published $H_{37}R_v$ reference genome. Among these was a large 2064-bp insertion (RvD6), which was originally detected in both $H_{37}R_a$ and CDC1551, but not $H_{37}R_v$.

* Corresponding author at: Mycobacteriology Research Centre, National Research Institute of Tuberculosis and Lung Disease (NRITLD), Shahid Beheshti University of Medical Sciences, Darabad, P.O. 19575/154, Tehran 19556, Iran.
E-mail address: pfarnia@hotmail.com (P. Farnia).

Peer review under responsibility of Asian African Society for Mycobacteriology.
http://dx.doi.org/10.1016/j.ijmyco.2015.12.001

*Conclusion:* Here, we show cell-wall free cells of MTB bacilli in their latent state, and the biological adaptation of these cells was more phenotypic in nature than genomic. These cell-wall free cells represent a good model for understanding the nature of TB latency.


## Introduction

Eradication of tuberculosis (TB) has been hampered partly by the ability of *Mycobacterium tuberculosis* (MTB) to remain dormant in the human body for years without causing disease, a state referred to as latent tuberculosis [1,2]. The shift of MTB into a persistent state can occur after initial infection (pre-antibiotic persistence) or after completion of TB treatment in patients who developed late reactivation (post-antibiotic persistence) [2–4]. Today, more than one-third of the world population (2.2 billion individuals) is estimated to harbor latent TB infection, of which 2–23% will develop active TB during their lifetime [5]. The reactivation process can be altered with HIV infection, malnutrition, drug use, cancer, diabetes, chronic renal insufficiency, and immunosuppressive drug therapy [3,5]. Therefore, more effort must be devoted to better control their progression and understand the latent state. In the last two decades, significant progress was made toward development and characterization of various aspects of latent TB cells [6–11]. However, our knowledge of these cells remains very limited, mainly due to their low numbers and our inability to precisely localize them in living host tissues. The existence of latent TB was originally recognized as non-culturable MTB living within closed pulmonary lesions [6,12]. The Cornell model of latency was the first experimental *in vivo* model providing evidence for latent TB bacilli [3,13]. Additionally, smear-negative autopsy specimens from asymptomatic humans were shown to induce active disease in animals, suggesting that MTB capable of causing disease can persist in a non-acid-fast, latent state [3,14,15]. Wayne [7] and Wayne and Hayes [16] proposed an *in vitro* model of MTB latency with two nonreplicating persistent (NRP) states: a microaerophilic ($NRP_1$) and a later anaerobic ($NRP_2$) state [7,16]. Overall, latency is believed to involve nonreplicating or very slow growing MTB [3,4,17]. The whole-genome sequence of laboratory strain MTB $H_{37}R_v$, and other clinical MTB isolates has enhanced our understanding of the genetic diversity among MTB strains, including the regulatory pathways that might contribute to stationary and persistent states [18,19]. Some of these pathways are specifically regulated during MTB persistence [3,4,20,21]; however, it is unclear whether these changes are heritable or special to the genome of MTB persister cells. Recently, we documented a morphological alteration of latent TB cells in $NRP_1$ and $NRP_2$ states of latency [22] that was similar to persister-like TB bacilli (size ranging from ~150 μm to 300 μm) observed in sputum from MDR-treated TB patients who experienced disease recurrence [23]. In the present investigation, we maintained $H_{37}R_V$ bacilli under oxygen- and nutrient-deprivation conditions for 782 days (26 months), followed by isolation and investigation of the cultured bacilli using light and atomic force microscopy (AFM; Nanoscope version 5.31R1), spoligotyping, and whole-genome sequencing. To our knowledge, this is the first report that provides detailed information about phenotypic and genomic characterization of persister MTB. We expect that the results of this study will provide fundamental information for understanding the biology, pathology, and treatment of latent tuberculosis.

## Materials and methods

### *Inoculation of MTB*

$H_{37}R_V$ cells at exponential growth phase [$OD_{600} = 0.05$ ($5 \times 10^6$ cfu/mL] were transferred to screw-cap test tubes (20 mm × 125 mm) containing low-nutrient Dubos medium [0.03% Tween and 10% Dubos albumin supplement without glycerol (Difco Laboratories Ltd., West Molesey, UK)] [8,20]. Magnetic stirrers were added to each tube, and the tubes were sealed using molten paraffin wax [22]. The culture tubes ($n = 10$) were constantly stirred (50–80 rpm) at 37 °C for 26 months. To isolate persister cells, cultures were centrifuged (14,000*g* for 30 min) to obtain cell pellets or sediments, which were passed through a 0.25-μm Millipore filter (EMD Millipore, Billerica, MA, USA). A smear prep for microscopic examination (Ziehl–Neelsen staining) was prepared for both filtered and unfiltered sediments. Sediments were also inoculated into both liquid (fresh 7H9-ADC-glycerol broth) and solid culture media (L.J & 7H10-Agar, blood agar) to determine whether cells were able to grow following the extended incubation (from 8 to 12 weeks). The culture tubes were read twice per week for 12 weeks.

### *Estimation of oxygen consumption*

Oxygen depletion was monitored via decolorization of the redox indicator methylene blue (1.5 μg/mL) in control tubes. The blue dye served as a visual indicator of hypoxia by fading and finally disappearing as oxygen was depleted [24].

### *AFM*

AFM images were recorded in contact mode using an optical-lever microscope equipped with a liquid cell (Nanoscope IV Multimode AFM; Veeco Metrology Group LLC, Santa Barbara, CA, USA). To image MTB on silicon plates, the surface was charged with polyclonal rabbit anti-mycobacterium antibody (B0124; Dako, Carpinteria, CA, USA) before adding 0.1 μL of diluted (1:10) MTB samples to the plate [25]. Both height and deflection images were recorded, using oxide-sharpened microfabricated $Si_3N_4$ cantilevers (Microlevers; Veeco Metrology LLC) with a spring constant of 0.01/nm [22,25]. Overall,

15–20 steel sample packs were used to observe each sample. The expected and observed frequencies of cell shape and cell size in different tube cultures were compared and analyzed by Fisher Exact test. The data presented here are the average of all observations.

### DNA extraction

Genomic DNA from filtered sediment was extracted using QIAamp DNA Mini Kit (Cat No: 51304; Qiagen, Hilden, Germany).

### Genotyping

Spoligotyping was performed according to the protocol described by Kamerbeek and colleagues [26].

### Genome sequencing and analysis

Illumina libraries were prepared and sequenced using the Illumina HiSeq2000 platform as previously described [27–29]. Sequence reads were mapped onto MTB $H_{37}R_V$ (GenBank accession number: CP003248.2) using BWA version 0.5.9.9 [27], and variants were identified using Pilon version 1.12 [28]. Sequence reads were also assembled using ALLPATHS-LG with Pilon correction as described for the Pilon-integrated tool [28]. Sequence reads and annotated assemblies were deposited into GenBank under BioSample ID SAMN02628494. Each Pilon-predicted variant was validated by manual inspection of read alignments to the $H_{37}R_V$ genome in IGV [27] and further assessed using the assembled genome. To detect larger events, such as insertions or rearrangements, the assembly was aligned to the $H_{37}R_V$ assembly using NUCmer in the MUMmer package [29]. Each assembly scaffold that did not perfectly match $H_{37}R_v$ was manually inspected and differences were reported. Only variable positions that were verified are described in the results. Finally, PROTEAN [30] was used to determine the effect of single nucleotide polymorphisms (SNPs) on protein function.

## Results

### Phenotypic changes

As previously reported [22], oxygen depletion was based on gradual hypoxia deprivation that was initially proposed by Wayne and Hayes [7,16]. However, in our model, MTB cells were starved for nearly ninefold longer than in previous experiments (782 vs. 90 days). The visual indicator of hypoxia, methylene blue, reported that the control culture tubes were hypoxic after 12–14 days of MTB inoculation, suggesting that during weeks 3–104 of incubation, the cells were starved of oxygen. At the end of 26 months (104 weeks), we prepared smears from the unfiltered sediments of all culture tubes (10 slides/per culture tube) and, using light microscopy, observed low numbers of acid-fast bacilli (AFB). We could not detect AFB on smears of the filtered sediments (suggesting that these cells could not pass through the 0.25-μm filter). Under AFM, the size and morphological appearance of cells differed between unfiltered and filtered sediments. A mixed population of rod-shaped (10–15%) or round (85–90%) cells with an average size of 1–0.5 μm were seen in unfiltered sediments from culture tubes (Fig. 1), whereas the filtered sediments consisted of uniformly oval or round-shaped cells with an average size of 0.1–0.3 μm (Figs. 2 and 3). When we subcultured cells from either filtered or unfiltered sediments, we did not observe growth in any culture media.

### Spoligotypes

The spoligotypes of the starting culture, $H_{37}R_v$ (ATCC25618), exhibited a pattern similar to that of the reference sequence (octal representation: 777777477760771) consisting of 43 spacers in the direct-repeat region [20]. The octal reading for the filtered sediments was 577757477760771, indicating that it was missing two spacers, i.e., 2 and 14 spacers as compared with the starting cultures.

### Whole-genome analysis

To identify differences between the NRITLD60 and $H_{37}R_v$ reference genomes, we used complimentary approaches that utilized the alignment of raw sequence reads from NRITLD60 and $H_{37}R_v$, and comparison of NRITLD60 and $H_{37}R_v$ whole-genome assemblies (Fig. 4). The NRITLD60 assembly consisted of 4,444,114 bases, had a G+C content of 65.57%, and was predicted to have 4057 genes (Table 1). Alignment of the NRITLD60 sequence to the $H_{37}R_v$ reference genome (accession number: CP003248.2) revealed that 99.98% of the $H_{37}R_v$ genome was represented in this strain, i.e., only the equivalent of ~880 bases were not represented in the NRITLD60 sequence, which is within the variability range observed between $H_{37}R_v$ strains globally [31]. In total, we identified eight variants that distinguished NRITLD60 from $H_{37}R_v$, including five SNPs, one large deletion, one three-base deletion, and one large insertion. We also detected seven additional variants that were less easy to verify, due to their being within high G+C-content regions of the genome, but may further distinguish these two strains, including three SNPs, two large insertions, one large deletion, and one large substitution. Of the eight total SNPs, four were nonsynonymous (RVBD_0516c; RVBD_1447c, RVBD_3080c, and RVBD_3479c), two were synonymous (RVBD_0633c and RVBD_3347c), and two were found within intergenic regions (RVBD_0049 and RVBD_0050). Using PROVEAN [30], we determined that only the nonsynonymous SNP in *zwf2* (RV1477c) was predicted to negatively impact protein function, while the three other SNPs were predicted to have a neutral effect. Deletions were observed within RV1755, RV452, and Rv2629 (Table 2). Deletions within RV1755 and RV452 were 617- and 26-bp in size, respectively, suggesting that these deletions alter protein function through frame shifts, likely inactivating the encoded protein. The other deletion observed in RV2629 was small (three bases) and did not cause a frame shift in the encoded gene, indicating its likely minimal impact on protein function. We also detected one large 2064-bp insertion in NRITLD60 at position 2,634,143 of the $H_{37}R_v$ genome. This insertion is designated as RvD6 and is located at the start codon of MRA_2373 (Rv2352c) [32].

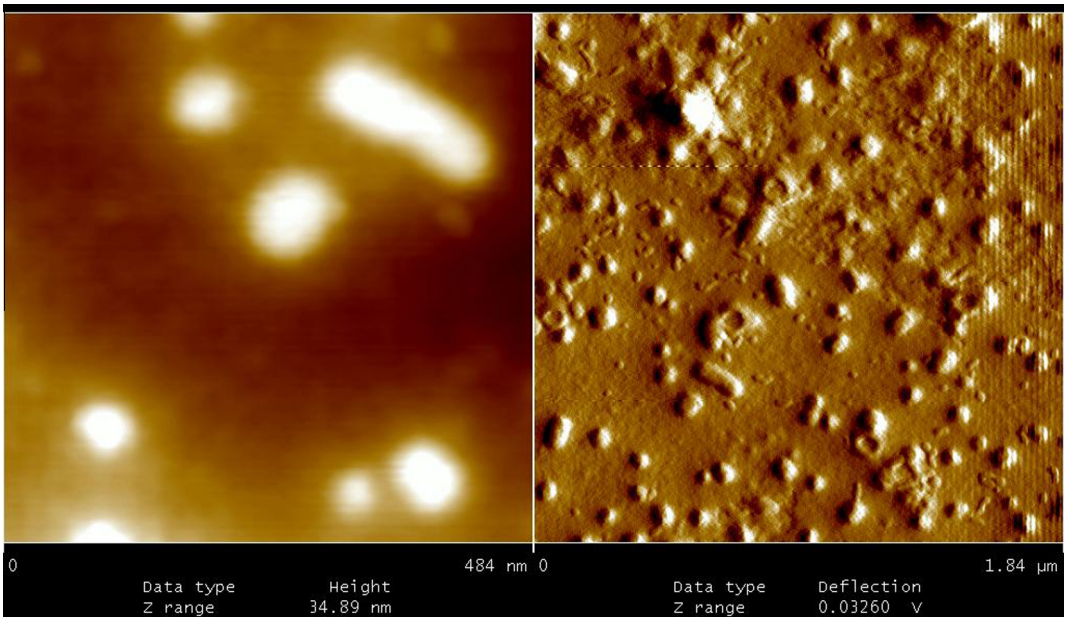


**Fig. 1 – Presence of rod and round shape cells in unfiltered sediments of MTB culture tubes after 782 days of oxygen and nutrient deprivation.**

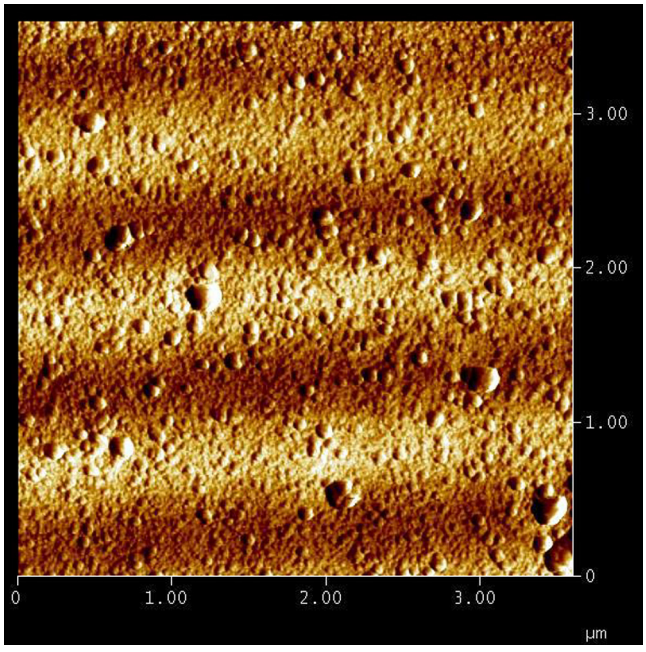


**Fig. 2 – Most of cells from filtered sediments of MTB cultures appeared to be round or oval shape.**

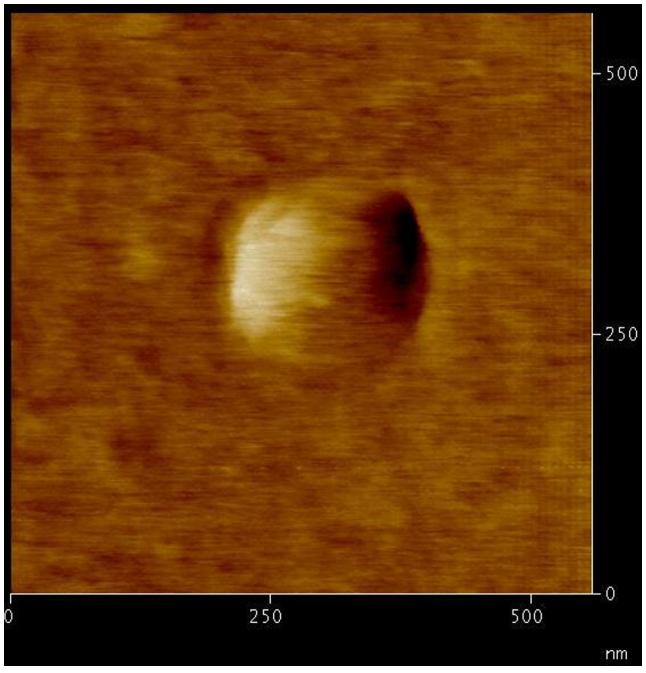


**Fig. 3 – The average size of "cell wall free" cells of latent MTB bacilli was ranging from 0.1 to 0.3 µm.**

## Discussion

The physiology, morphology, and genetic characterization of latent MTB are incompletely explored. During TB latency, MTB are restricted to the characteristic TB lesions, where they enter into a quiescent state and survive for extended periods of time. Robertson [33] and Feldman and Baggenstoss [15] were among the first to show that passage of infected tissues from asymptomatic patients to animals induced TB infection [15,33], despite the lack of AFB in these tissues. This observation prompted a debate concerning the physiological and morphological characteristics of latent MTB [3–10]. Some proposed that bacilli entered into an altered developmental state in which acid fastness was lost, while others suggested that acid fastness was retained and that the number of bacilli was too low for microscopic detection [34,35]. Here, we used a double-deprivation model for latency and detected a heterogeneous population of cells after a 26-month incubation

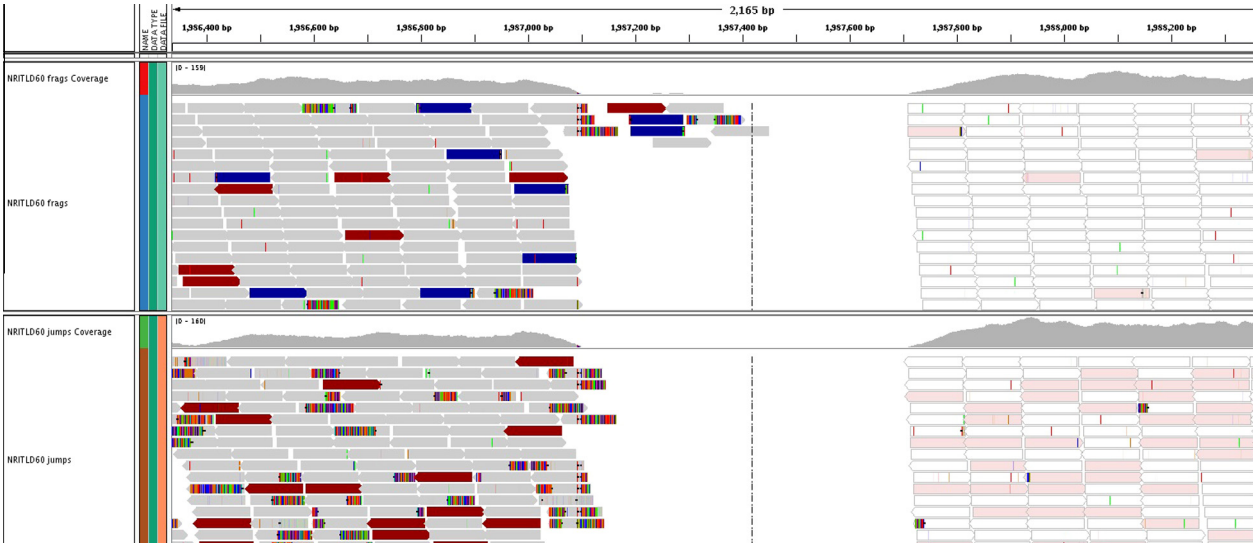


**Fig. 4 – Reads from two NRITLD60 libraries ("NRITLD60 frags" and "NRITLD60 jumps") aligned to a ~2 kb region of $H_{37}R_v$ (base position 1,986,400 to 1,988,400) are shown in IGV [47]. Beginning at roughly 1,987,100 and until base position 1,987,711, there is a dropout in aligned coverage in both the fragment and jump reads thus illustrating the 616 base deletion reported by Pilon (1,987,095–1,987,711).**

consisting of few acid-fast and many non-acid-fast bacilli (Figs. 1–3). Therefore, the observed AFB were most likely dead bacilli, as subculturing of these cells resulted in no growth in liquid or solid culture media. Using high-resolution AFM, we also observed that the filtered MTB culture media was densely populated with non-acid-fast bacilli. Cell-wall deficient forms of MTB have been proposed for decades [34–36], but these cell types have never been visualized or described [3,32–34]. Here, we were able to isolate and visualize these cells by filtering cultures and binding filtered cells to a silicon surface coated with polyclonal rabbit anti-MTB. As shown in Figs. 2–4, these cells were round or oval in shape with an average size of 150–300 μm. Generally, microorganisms begin to adapt by changing their shape and reducing their size [37,38]. In this regard,

**Table 1 – Whole-genome assembly of NRITLD60.**

| Name | G57704 all paths 100f50j 49443 |
|---|---|
| Assembler | All paths |
| Contigs | 73 |
| Max contig | 305,125 |
| Mean contig | 60,831 |
| Contig N50 | 109,043 |
| Contig N90 | 48,018 |
| Total contig length | 4,440,670 |
| Assembly GC | 65,577 |
| Scaffolds | 68 |
| Max scaffold | 305,125 |
| Mean scaffold | 65,355 |
| Scaffold N50 | 136,972 |
| Scaffold N90 | 54,577 |
| Total scaffold length | 4,444,114 |
| Captured gaps | 5 |
| Max gap | 2119 |
| Mean gap | 687 |
| Gap N50 | 2119 |
| Total gap length | 3436 |

mycobacteria, similar to other bacteria, depend upon the laws of diffusion to bring compounds to their surface to enable their mixing with macromolecules in the cytoplasm [37–39]. Therefore, to import nutrients in harsh environments, MTB increases their surface area without increasing the surface-to-volume ratio [37,39], which can occur when mycobacterium changes from a rod to a round shape [37]. Overall, the theory of morphological alteration in MTB species has been discussed by many investigators, but it has not been definitively proven [34,35,40]. For example, Mitchison et al. [41] used the Cornell model of latency to show that homogenate-tissue biopsies from sterile mice were positive for MTB DNA [41], though MTB positivity based on polymerase chain reaction has been argued to result from the presence of dead microorganisms [42]. In our study, the isolated non-acid- fast bacilli were identified as MTB by spoliogtyping and whole-genome sequencing. Spoligopatterns were identical to standard $H_{37}R_v$, but spacers 2 and 14, as well as spacers 20 and 21 and 33 through 36, were missing. The genome was also very similar to $H_{37}R_v$, with only 15 differences detected. Among the observed variations, one nonsynonymous SNP in RVBD147c was predicted to negatively impact encoded protein function. Normally, the *Zwf* gene encodes glucose-6-phosphate dehydrogenase (G6PDH), an enzyme that catalyzes NAD+ or NADP+-dependent conversion of glucose-6-phosphate to 6-phosphogluconate [43]. The activity of G6PDH and *zwf* is maximal in early logarithmic phase and dramatically reduced when bacteria approach stationary phase [44]. The detected SNP at codon 248 (aAc to aTc) of *zwf2* resulted in an asparagine-to-isoleucine change in the *zwf2*-encoded protein, which might play an important role in shifting *zwf* transcription during latency [44]. We also found one large insertion at position 2,634,143 in $H_{37}R_v$ using an assembly-based method. This insertion, which is designated RvD6, consists of 2064 bp and is present in both $H_{37}R_a$ and CDC1551, but is deleted from $H_{37}R_v$ [32]. This fragment

**Table 2 – Deletions within RV1755 and RV452.**

| Deletion segment RV ID; gene name | Codon position | Gene length | Protein length | Product | Function | Functional category |
|---|---|---|---|---|---|---|
| RV2629 | 527, codon_pos: 2:AAC | 1,125 | 374 | Conserved protein | Function unknown | Conserved hypothetical |
| RV1755c; *plcD* | 591, codon_pos:3, codon: CGC | 843 | 280 | Probable phospholipase C 4 (fragment); PlcD | Hydrolyzes sphingomyelin and phosphatidylcholine. Probable virulence factor implicated in the pathogenesis of *Mycobacterium tuberculosis* at the level of intracellular survival by the alteration of cell-signaling events or by direct cytotoxicity. | Intermediary metabolism and respiration |
| Rv1450c | 1,090, codon_pos: 1:GGC | 3,990 | 1,329 | Function unknown | PE-PGRS family protein PE_PGRS27 | PE/PPE |

*Note:* ID = identification; PE = proline–glutamate motif; PGRS = polymorphic GC-rich sequence; PPE = proline–proline–glutamate motif.

contains two genes (MRA_2374 and MRA_2375) encoding an Esat-6-like protein, and a gene encoding a PPE-family protein (MRA_2376) located at the start codon of MRA_2373 (Rv2352c) [32].

The presence of this insertion is interesting and needs further investigation. In this study, we used the Wayne model of latency, which resulted in the gradual self-generated oxygen depletion of MTB cultures grown in sealed tubes [7,16]. Upon the slow shift of aerobic-growing MTB to anaerobic conditions in the presence of low or zero nutrients, the cultures were able to adapt and survive anaerobiosis by shifting to a state of NRP [3,7,16]. This anaerobic condition is similar to that of hypoxia observed within the necrotic material of TB lesions, where bacterial latency is known to occur [3,17,24]. In this situation, we might expect a similar morphological adaption of MTB cells in human host tissue. Thus, it may be more reliable to investigate the presence of cell-wall free cells in latent TB patients rather than to look for AFB. Finally, if we are willing to accept the presence of cell-wall free latent MTB cells, then newer strategies to prevent their progression should be highlighted. Currently, World Health Organization guidelines for the management of latent TB are only available for people with HIV and for children <5 years of age who have household contact with TB cases [45]. This treatment protocol is mainly based on isoniazid (INH) therapy. INH is a pro drug that inhibits the synthesis of mycolic acid required for the mycobacterial cell wall. As we showed, filtered latent MTB bacilli lack cell-wall components; therefore, it is difficult to explain how INH monotherapy can be effective during latency. It may be possible that INH monotherapy would not kill latent cells, but would prevent their growth. Recently, a new regimen called the 12-dose regimen was proposed by Centers for Disease Control [46]. This regimen reduces treatment from 270 doses given daily for 9 months to 12 once-weekly doses given for 3 months using a combination of isoniazid and rifapentine. Based on our study, it seems that the 12-dose regimen may be more effective than monotherapy with INH. In summary, cell-wall free latent MTB bacilli were characterized both at the genomic and cellular levels. The information provided in this study may help resolve questions regarding the nature of MTB cells in their latent state. A limitation in the interpretation of our results is that direct comparisons should have been made between the induced latent organisms and those in the starting culture. However, this does not detract from the important observation that large numbers of organisms in the latent state lack a cell wall. Therefore, the potential impact of this on future treatment of patients with latent infection must be taken into account.

## Conflicts of interest

The authors declare no conflicts of interest.

## Acknowledgments

The authors are grateful to the Mycobacteriology Research Center (NRITLD), Tehran, and the Microbiology Department within the Republican Research and Practical Centre of Minsk for their help and cooperation.

This study was sponsored by the Ministry of Health, Medical Education, Deputy of Research (2009–2010) and the National Research Institute of TB and Lung Diseases (NRITLD), Tehran, Iran. This project was also funded in part with federal funds from the National Institute of Allergy and Infectious Diseases (NIAID), National Institutes of Health, and Department of Health and Human Services under contract number: HHSN272200900018C and Grant number U19AI110818 awarded to the Broad Institute.

## REFERENCES

[1] J.R. Amberson, The significance of latent forms of tuberculosis, N. Engl. J. Med. 219 (1938) 5726.
[2] J.L. Flynn, J. Chan, Tuberculosis: latency and reactivation, Infect. Immun. 69 (2001) 4195–4201.
[3] N.M. Parrish, J.D. Dick, W.R. Bishai, Mechanisms of latency in mycobacterium tuberculosis, Trends Microbiol. 107 (1998) 110–112.
[4] P.J. Cardona, J. Ruiz Manzano, On the nature of *Mycobacterium tuberculosis*-latent bacilli, Eur. Respir. J. 24 (2004) 1044–1051.
[5] World Health Organization (WHO), Global tuberculosis reports, <http://www.who.int/tb/publication/global_report/en> (Last accessed on 01.03.14).
[6] H.J. Corper, M.L. Cohn, The viability and virulence of old cultures of tubercle bacilli: studies on 12-year broth cultures maintained at incubator temperature, Ann. Rev. Tuberc. 28 (1933) 856–887.
[7] L.G. Wayne, Dynamics of submerged growth of *Mycobacterium tuberculosis* under aerobic and microaerophilic conditions, Am. Rev. Respir. Dis. 114 (1976) 807–811.
[8] M. Gengenbacher, S.P.S. Rao, K. Pethe, et al, Nutrient-starved, nonreplicating *Mycobacterium tuberculosis* requires respirations, ATP synthase, and isocitrate lyase for maintenance of ATP homeostasis and viability, Microbiology 156 (2010) 81–87.
[9] M.O. Shleeva, Y.K. Kudykina, G.N. Vostroknutova, et al, Dormant ovoid cells of *Mycobacterium tuberculosis* are formed in response to gradual external acidification, Tuberculosis 91 (2011) 146–154.
[10] A.F. Cunningham, C.L. Spreadbury, Mycobacterial stationary phase induced by low oxygen tension: cell-wall thickening and localization of the 16-kilodalton α-homolog, J. Bacteriol. 180 (1998) 801–808.
[11] A.S. Kaprelyants, J.C. Gottschal, D.B. Kell, Dormancy in nonsporulating bacteria, FEMS Microbiol. Rev. 10 (1993) 271–285.
[12] T.R. Rustad, A.M. Sherrid, K.J. Minch, et al, Hypoxia: a window into *Mycobacterium tuberculosis* latency, Cell. Microbiol. 11 (2009) 1151–1159.
[13] R.M. McCune, F.M. Feldmann, H.P. Lambert, et al, Microbial persistence. I. The capacity of tubercle bacilli to survive sterilization in mouse tissues, J. Exp. Med. 123 (1966) 445–468.
[14] R.M. McCune, R. Tompsett, W. McDermott, The fate of *Mycobacterium tuberculosis* in mouse tissues as determined by the microbial enumeration technique. II. The conversion of tuberculous infection to the latent state by the administration of pyrazinamide and a companion drug, J. Exp. Med. 104 (1957) 763–802.
[15] W.H. Feldman, A.H. Baggenstoss, The occurrence of virulent tubercle bacilli in presumably non-tuberculous lung tissue, Am. J. Pathol. 15 (1939) 501–515.
[16] L.G. Wayne, L.G. Hayes, An *in vitro* model for sequential study of shiftdown of *Mycobacterium tuberculosis* through two stages of nonreplicating persistence, Infect. Immun. 64 (1996) 2062–2069.
[17] T. Kondratieva, T. Azhikina, B. Nikonenko, et al, Latent tuberculosis infection: what we know about its genetic control?, Tuberculosis 94 (2014) 462–468
[18] S.T. Cole, R. Brosch, J. Parkhill, et al, Deciphering the biology of *Mycobacterium tuberculosis* from the complete genome sequence, Nature 393 (1998) 537–544.
[19] V. Periwa, A. Patowary, S.K. Vellarikkal, et al, Comparative whole-genome analysis of clinical isolates reveals characteristic architecture of *Mycobacterium tuberculosis* pangenome, PLoS One 10 (2015) e0122979.
[20] C. Deb, C.M. Lee, V.S. Dubey, et al, A novel *in vitro* multiple-stress dormancy model for *Mycobacterium tuberculosis* generates a lipid-loaded, drug-tolerant, dormant pathogen, PLoS One 4 (2009) e6077.
[21] L.M. Verhagen, A. Zomer, M. Maes, et al, A predictive signature gene set for discriminating active from latent tuberculosis in Warao Amerindian children, BMC Genomics 14 (2013) 74–85.
[22] A.A. Velayati, P. Farnia, M.R. Masjedi, et al, Sequential adaptation in latent tuberculosis bacilli: observation by atomic force microscopy, Int. J. Clin. Exp. Med. 4 (2011) 193–199.
[23] A.A. Velayati, P. Farnia, M.R. Masjedi, Recurrence after treatment success in pulmonary multidrug-resistant tuberculosis: predication by continual PCR positivity, Int. J. Clin. Exp. Med. 5 (2012) 271–272.
[24] A. Lim, M. Eleuterio, B. Hutter, et al, Oxygen depletion-induced dormancy in *Mycobacterium bovis* BCG, J. Bacteriol. 181 (1999) 2252–2256.
[25] G. Zhavnerko, N.N. Poleschuyk, Mycobacterium under AFM tip: advantages of polyelectrolyte-modified substrate, Int. J. Myobacteriol. 1 (2012) 53–56.
[26] J. Kamerbeek, L. Schouls, A. Kolk, et al, Simultaneous detection and strain differentiation of *Mycobacterium tuberculosis* for diagnosis and epidemiology, J. Clin. Microbiol. 35 (1997) 907–914.
[27] H. Li, R. Durbin, Fast and accurate short read alignment with Burrows–Wheeler transform, Bioinformatics 25 (2009) 1754–1760.
[28] B.J. Walker, T. Abeel, T. Shea, et al, Pilon: an integrated tool for comprehensive microbial variant detection and genome assembly improvement, PLoS One 9 (2014) e112963.
[29] A.L. Delcher, S.L. Salzberg, A.M. Phillippy, Using MUMmer to identify similar regions in large sequence sets, Curr. Protoc. Bioinformatics (2003), http://dx.doi.org/10.1002/0471250953.bi1003s00 (Chapter 10).
[30] Y. Choi, G.E. Sims, S. Murphy, et al, Predicting the functional effect of amino acid substitutions and indels, PLoS One 7 (2012) e46688.
[31] T.R. Ioerger, Y. Feng, K. Ganesula, et al, Variation among genome sequences of H37Rv strains of Mycobacterium tuberculosis from multiple laboratories, J. Bacteriol. 192 (2010) 3645–3653.
[32] H. Zheng, L. Lu, B. Wang, et al, Genetic basis of virulence attenuation revealed by comparative genomic analysis of *Mycobacterium tuberculosis* strain H37Ra versus H37Rv, PLoS One 3 (2008) e2375.
[33] H.E. Robertson, The persistence of tuberculous infections, Am. J. Pathol. 9 (1933) 711–718.
[34] A.G. Khomenko, The variability of *Mycobacterium tuberculosis* in patients with cavitary pulmonary tuberculosis in the course of chemotherapy, Tubercle 68 (1987) 243–245.
[35] J.L. Stanford, Much's granules revisited, Tubercle 68 (1987) 241–242.
[36] H. Much, Uber die granuläre, nach Ziehl nicht färbbare forms des tuberkulose virus, Beiträge zur Klinik der Tuberkulose 8 (1907) 85.

[37] K.D. Young, The selective value of bacterial shape, Microbiol. Mol. Biol. Rev. 70 (2006) 660–703.
[38] A.A. Velayati, P. Farnia, Shape variation in *Mycobacterium tuberculosis*, Iran J. Clin. Infect. Dis. 6 (2011) 95–101.
[39] T.J. Beveridge, The bacterial surface: general considerations towards design and function, Can. J. Microbiol. 34 (1988) 363–372.
[40] A.L. Koch, What size should a bacterium be? a question of scale, Annu. Rev. Microbiol. 50 (1996) 317–348.
[41] D. de Wit, M. Wootton, J. Dhillon, et al, The bacterial DNA content of mouse organs in the Cornell model of dormant tuberculosis, Tubercle Lung Dis. 76 (1995) 555–562.
[42] R. Hernández-Pando, M. Jeyanathan, G. Mengistu, et al, Persistence of DNA from *Mycobacterium tuberculosis* in superficially normal lung tissue during latent infection, Lancet 356 (2000) 2133–2138.
[43] J.M. Sandoval, F.A. Arenas, C.C. Vásquez, Glucose-6-phosphate dehydrogenase protects Escherichia coli from tellurite-mediated oxidative stress, PLoS One 6 (2011) e25573.
[44] J.M.N. Liorens, A. Tormo, E. Martínez-García, Stationary phase in gram-negative bacteria, FEMS Microbiol. Rev. 34 (2010) 476–495.
[45] World Health Organization, Guidelines on the management of latent tuberculosis infection, <http://www.who.int/tb/publications/ltbi_document_page/en/>, 2015 (accessed 25.11.14).
[46] Centers for Disease Control and Prevention, Recommendations for use of an isoniazid–rifapentine regimen with direct observation to treat latent Mycobacterium tuberculosis infection, MMWR Morb. Mortal. Wkly Rep. 60 (2011) 1650–1653.
[47] J.T. Robinson, H. Thorvaldsdóttir, W. Winckler, et al, Integrative genomics viewer, Nat. Biotechnol. 29 (2011) 24–26.